We are IntechOpen, the world's leading publisher of Open Access books
Built by scientists, for scientists

6,900
Open access books available

186,000
International authors and editors

200M
Downloads

Our authors are among the

154
Countries delivered to

TOP 1%
most cited scientists

12.2%
Contributors from top 500 universities

Interested in publishing with us?
Contact book.department@intechopen.com

Numbers displayed above are based on latest data collected.
For more information visit www.intechopen.com

The Deformability and Microstructural Aspects of Recrystallization Process in Hot-Deformed Fe-Ni Superalloy

Kazimierz J. Ducki
Silesian University of Technology
Poland

1. Introduction

The behaviour of metals and alloys during hot plastic working has a complex nature and it varies with the changing of such process parameters as (Zhou et al., 1994): deformation, strain rate and temperature. The high-temperature plastic deformation is coupled with dynamic recovery and recrystallization processes which influencing the structure and properties of alloys. One of crucial issues is finding the relationship between the hot plastic deformation process parameters, microstructure and properties. Since the sixties of the last century, theoretical and experimental investigations have been carried out to find those interdependence for steels and nickel alloys.

In the recent years, the constitutive equations describing hot plastic deformation processes have started to take into account the so-called internal variables determining the material condition. These variables include substructural parameters such as (Hansen, 1998; Sellars, 1998): grain size, grain shape, recrystalized volume fraction, dislocation density, subgrain size, subgrain misorientation angle and stacking fault energy (SFE). Determination of the above-mentioned parameters of a deformed material structure description requires the application of analytical methods primarily based on quantitative metallography and transmission electron microscopy (TEM). Taking those substructure parameters into consideration in calculations should enable the correct modelling of structural phenomena during hot plastic deformation and enhance the technological processes control for the purpose of obtaining the assumed structures of required properties (McQeen et al., 2002).

The Fe-Ni superalloys precipitation hardened by intermetallic phase of γ' - Ni$_3$(Al,Ti) type are one of the groups of construction materials intended for operation in cryogenic and elevated temperatures. These alloys are difficult to deform and are characterized by high values of yield stress at a high temperature. High deformation resistance of Fe-Ni alloys is caused by a complex phase composition, high activation energy of the hot plastic deformation process and a low rate of dynamic recrystallization. When choosing the conditions for hot plastic working of Fe-Ni alloys, the following factors should be considered (Bywater et al., 1976; Kohno et al., 1981; Ducki et al., 2006): the matrix grain size, plastic deformation parameters and the course of the recrystallization process. The grain size is of particular importance. Grain refining leads to an increased rate of recovery and

dynamic recrystallization and to a smaller diameter of recrystallized grains. This is important, for the grain refinement in Fe-Ni superalloys has an advantageous influence on increasing their yield point and fatigue strength (Koul et al., 1994; Härkegård et al., 1998).

In the presented study, research has been undertaken on the influence of the initial microstructure of austenite and the parameters of hot plastic working on deformability, grain and subgrain size, and dislocation density in a high-temperature creep resisting Fe-Ni alloy. It is assumed that the results obtained will be used for optimizing hot plastic working processes and forecasting the microstructure and functional properties of products made of Fe-Ni superalloys.

2. Material and methodology

The examinations were performed on rolled bars, 16 mm in diameter, of an austenitic A-286 type alloy. The chemical composition is given in Tab. 1.

Content of an element [wt. %]															
C	Si	Mn	P	S	Cr	Ni	Mo	V	W	Ti	Al	Co	B	N	Fe
0.05	0.56	1.5	0.026	0.016	14.3	24.5	1.35	0.42	0.10	1.88	0.16	0.08	0.007	0.0062	55.3

Table 1. Chemical composition of the investigated Fe-Ni superalloy

In order to model the conditions of alloy heating prior to plastic processing, the investigations were carried out on samples after initial soaking at high temperatures. Sections of rolled bars, which the samples for investigations were made of, were subjected to two variants of preheating, i.e. 1100°C/2h and 1150°C/2h with subsequent cooling in water. Heat treatment of this type corresponds to the soaking parameters of the investigated superalloy before hot plastic processing (Kohno et al., 1981).

The research on the alloy deformability was performed in a hot torsion test on a Setaram torsion plastometer 7 MNG. The plastometric tests were performed every 50°C in a temperature range of 900÷1150°C, with a constant holding time of 10 minutes at the defined temperature. Solid cylindrical specimens (Ø 6.0 × 50 mm) were twisted at a rotational speed of 50 and 500 rpm, which corresponds to the strain rate of 0.1 and 1.0 s⁻¹, respectively. To freeze the structure, the specimens after deformation until failure were directly rapid cooled in water (Fig. 1).

The data obtained in the plastometric torsion test were entered in an Excel spreadsheet in the form of columns containing the recorded values. Processing of the measured data by means of filtration, cutting, shrinking and planishing was conducted using the Matlab 6 program. A correction of the torque moment, due to diversified rotational speed values and increase of the sample temperature during torsion, was calculated by the method of joint action of speed and temperature from the following relations (Hadasik, 2005):

$$M''' = M + \Delta M''' \tag{1}$$

$$\Delta M''' = M(N, \dot{N}, T) - M(N, \dot{N}_r, T + \Delta T) \tag{2}$$

$$\Delta M''' = A \cdot N^B \cdot \exp(C \cdot N) \cdot \dot{N}^{D+\frac{E}{T}} \cdot \exp\left(\frac{F}{T}\right) - A \cdot N^B \exp(C \cdot N) \cdot \dot{N}^{D+\frac{E}{T+\Delta T}} \cdot \exp\left(\frac{F}{T+\Delta T}\right) \quad (3)$$

where: M – recorded torque moment [Nm]; M''' – corrected torque moment value [Nm]; $\Delta M'''$ – torque moment correction taking account of a joint action of speed and temperature [Nm]; N – number of sample torsion, $\dot{N}$ – given torsion speed [rpm]; $\dot{N}_r$ – recorded rotational speed [rpm]; T – deformation temperature [°C]; ΔT – temperature increment during torsion [°C]; A, B, C, D, E, F – material constans.
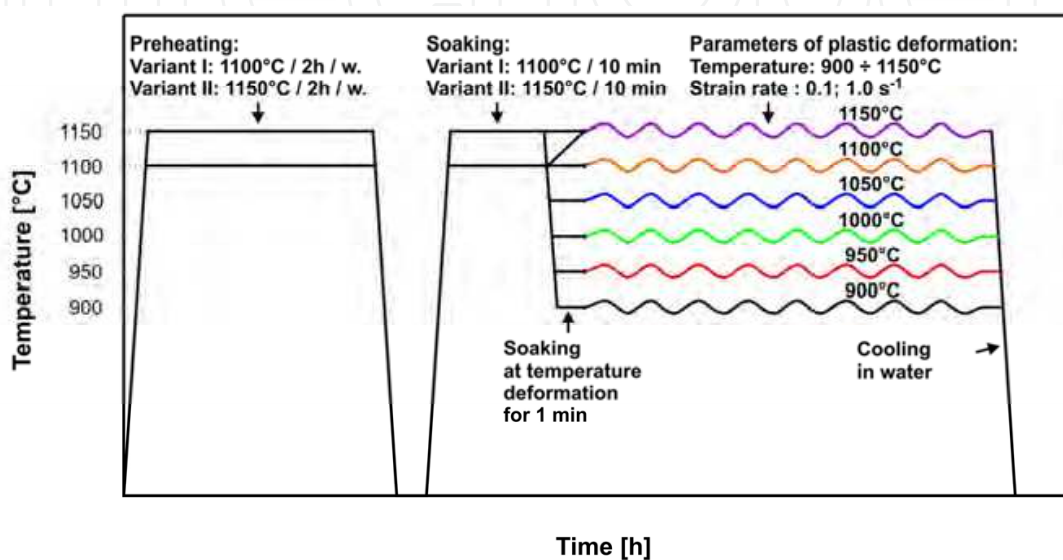
Fig. 1. Scheme of plastometric examination of the Fe-Ni alloy

The corrected data constituted a basis for the determination of equivalent deformation ε as a function of the number of the sample's rotations during torsion (Hadasik, 2005):

$$\varepsilon = \frac{2}{\sqrt{3}} \times \arcsin h\left(\frac{\pi \overline{R} N}{L}\right) \quad (4)$$

where: $\overline{R}$ equivalent radius corresponding to 2/3 of the outer radius R of the sample, L – measured sample length.

Yield stress σ_p was determined according to relation (5) taking account of the corrected torque moment M''', sample radius R, parameters m, p and axial force F_o (Hadasik, 2005):

$$\sigma_p = \left[\left(\frac{\sqrt{3} \cdot M'''}{2\pi R^3}\right)^2 \times (3+p+m)^2 + \left(\frac{F}{\pi R^2}\right)^2\right]^{0,5} \quad (5)$$

where: p – parameter reflecting stress sensitivity to deformation size; m – parameter reflecting stress sensitivity to deformation rate.

On the flow curves determined, the following parameters characterising plastic properties of the alloy in the torsion test were defined:

- σ_{pp} – maximum yield stress on the flow curve;
- ε_p – deformation corresponding to the maximum yield stress;
- σ_f – stress at which the sample is subject to failure;
- ε_f – deformation at which the sample is subject to failure, the so-called threshold deformation.

Relations between the yield stress and alloy deformation, and the deformation conditions were described using the Zener-Hollomon parameter Z (Zener et al., 1944):

$$Z = \dot{\varepsilon} \times \exp\left(\frac{Q}{RT}\right) = A \times \left[\sinh\left(\alpha\sigma_{pp}\right)\right]^n \tag{6}$$

where: $\dot{\varepsilon}$ – strain rate, Q – activation energy of the hot plastic deformation process, R – molar gas constant, T – temperature, and A, α, n – constants depending on grade of the investigated material.

The activation energy of the hot plastic deformation process Q was determined in accordance with the procedure specified in the work by (Schindler et al., 1998). The solution algorithm consisted in transforming equation (6) to the following form:

$$\dot{\varepsilon} = A \times \exp\left(\frac{-Q}{RT}\right)\left[\sinh(\alpha\sigma_{pp})\right]^n \tag{7}$$

Further procedure was based on solving equation (7) by a graphic method with the application of a regression analysis.

Structural inspections were performed on longitudinal microsections taken from the plastically deformed samples until failure after so-called "freezing" (Fig. 2). The specimens were etched using a reagent: 54 cm³ HF, 8 cm³ HNO$_3$ and 38 cm³ distilled H$_2$O. Due to the deformation inhomogeneity, microscopic observation was conducted in a representative region located at a distance of ca. 0,65÷0,75 of the specimen radius.

cutting line   3   2   1
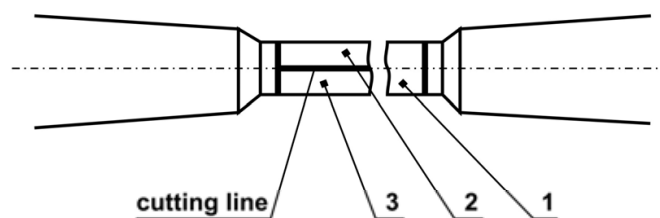
1 - transverse microsection to axis sample
2 - longitudinal microsection to axis sample
3 - thin foil

Fig. 2. Scheme of material cutting for metallographic microsections and thin foils from plastometric samples

A quantitative analysis of the investigated structures was carried out by means of a computer program MET-ILO v. 3.0 (Szala, 1997). For the analyzed microstructures, in accordance with the methodology presented in paper (Cwajna et al., 1993), the following stereological parameters were determined:

- average area of grain plane section $\bar{A}$ [μm²]:

$$\bar{A} = \frac{1}{N_A}$$ (8)

where: N_A – average grains number on area unit [μm⁻²];

- variability coefficient of the grain plane section area $v(A)$:

$$v(A) = \frac{S(A)}{\bar{A}} \times 100 \, [\%]$$ (9)

where: $S(A)$ – empirical standard deviation of grain section area;

- volume fraction of dynamically recrystallized grains in the structure V_V [%];
- grain elongation coefficient δ (Feret coefficient):

$$\delta = \frac{F_x}{F_y}$$ (10)

where: $F_{x,y}$ – Feret diameters in x and y axes direction;

- classical, dimensionless shape coefficient ξ:

$$\xi = \frac{4\pi\bar{A}}{P^2}$$ (11)

where: P – perimeter of grain plane section.

The examination of the substructure was carried out by means of a JEM-100B Joel transmission electron microscope. Direct measurements on the TEM micrographs allowed the calculation of the structural parameters: the average subgrain area $\bar{A}$, and the mean dislocation density ρ. The mean subgrain areas were determined by a planimetric method making use of a semi-automatic image analyser MOP AMO 3 type. The measurements were conducted on the TEM images. The analysed microsections of thin foils involved measurements of about 150 subgrains for each sample. The mean dislocation density was calculated by use of a method based on counting the inter-section points of a network superimposed over the micrograph with dislocation lines. The dislocation density ρ as calculated for the thin foils according to the relation (Klaar et al., 1992):

$$\rho = \frac{x \cdot (n_1 / l_1 + n_2 / l_2)}{t} \quad [\text{m}^{-2}]$$ (12)

where: x – a coefficient which defines the fraction of invisible dislocations with Burgers vectors $a/2<111>$ for the A1 structure: $x = 2$ for image of dislocations observed in (111) reflex, $x = 1.5$ for image of dislocations observed in (200) reflex, $x = 1.5$ for image of dislocations observed in (220) reflex; $l_{1(2)}$ – the total length of the horizontal (vertical) lattice lines; $n_{1(2)}$ – the number of intersections of the horizontal (vertical) lattice lines with dislocations; t – the thickness of the foil.

The thickness of the foil in the investigated areas can be approximately calculated following the formula (Head et al., 1973):

$$t = n \cdot \zeta_{hkl} \qquad (13)$$

where: n – a number of extinction lines; ζ_{hkl} – a value of extinction.

The values of ζ_{hkl} given by (Head et al., 1973) must be considered as a rough estimation of the actual value of extinction for the investigated material.

3. Results and discusion

3.1 Initial microstructure of the alloy

The application of two variants of initial solution heat treatment simulating the heating conditions allowed diversifying significantly the initial microstructure of the Fe-Ni alloy before hot plastic deformation. The alloy in its initial state differed primarily in the average grain size. After solution heat treatment under the conditions of 1100°C/2h/w., in the alloy microstructure presence was found of twinned austenite with medium-size grain ($\bar{A}$ = 2120 μm²) with a small amount (ca. 0.3 wt.%) of insoluble particles (Fig. 3a). The increasing of the solution heat treatment temperature to 1150°C at an analogous soaking time resulted in an increase of the austenite grain ($\bar{A}$ = 6296 μm²) and a reduction in the quantity and size of undissolved primary particles (Fig. 3b). For the analyzed variants of solution heat treatment, the microstructure of the samples was characterized by equiaxial grains, as evidenced by the elongation coefficient δ approximate to 1 and the dimensionless shape factor ξ of approximately 0.6.

Presence of titanium compounds, such as TiC carbide, $TiN_{0.3}$ nitride, $TiC_{0.3}N_{0.7}$ carbonitride, $Ti_4C_2S_2$ carbosulfide and Lavesa Ni_2Si phase and boride MoB was disclosed in the phase composition of the undissolved particles (Ducki, 2010).
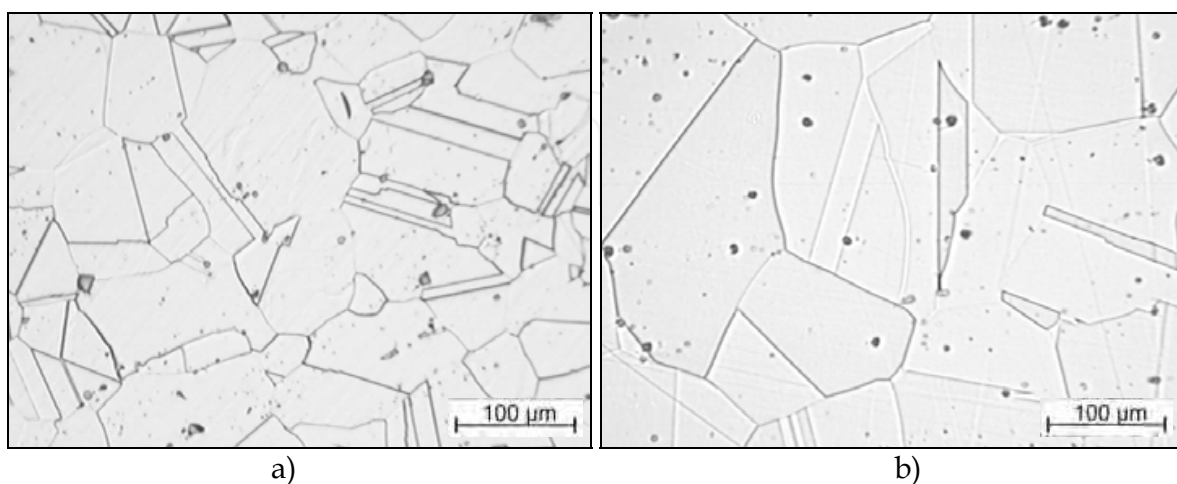
Fig. 3. Diversified microstructure of alloy after solution heat treatment at: a) 1100°C/2 h/w., $\bar{A}$ = 2120 μm²; b) 1150°C/2 h/w., $\bar{A}$ = 6296 μm²

3.2 Deformability of the alloy

Knowledge of the phenomena occurring during hot deformation of materials enables selecting the correct conditions for plastic working and shaping their material characteristics. The results of the plastometric investigations, in the form of the calculated alloy flow curves at temperatures of 900÷1150°C for two options of initial soaking are shown in Fig. 4 and 5. The curves obtained for the option of initial soaking at 1100°C/2h and strain rate 0.1 s^{-1} have a shape characteristic of a material in which dynamic recovery and recrystallization take place (Fig. 4). High deformation values were obtained for the alloy in a wide range of torsion temperatures, i.e. 950÷1100°C. An increase of strain rate to 1.0 s^{-1} results in a significant increase of yield stress values and a distinct decrease of the alloy deformability at all temperatures analysed. This phenomenon can be explained by a higher alloy consolidation rate as well as too slow removal of the reinforcement as a result of dynamic recovery and recrystallization.
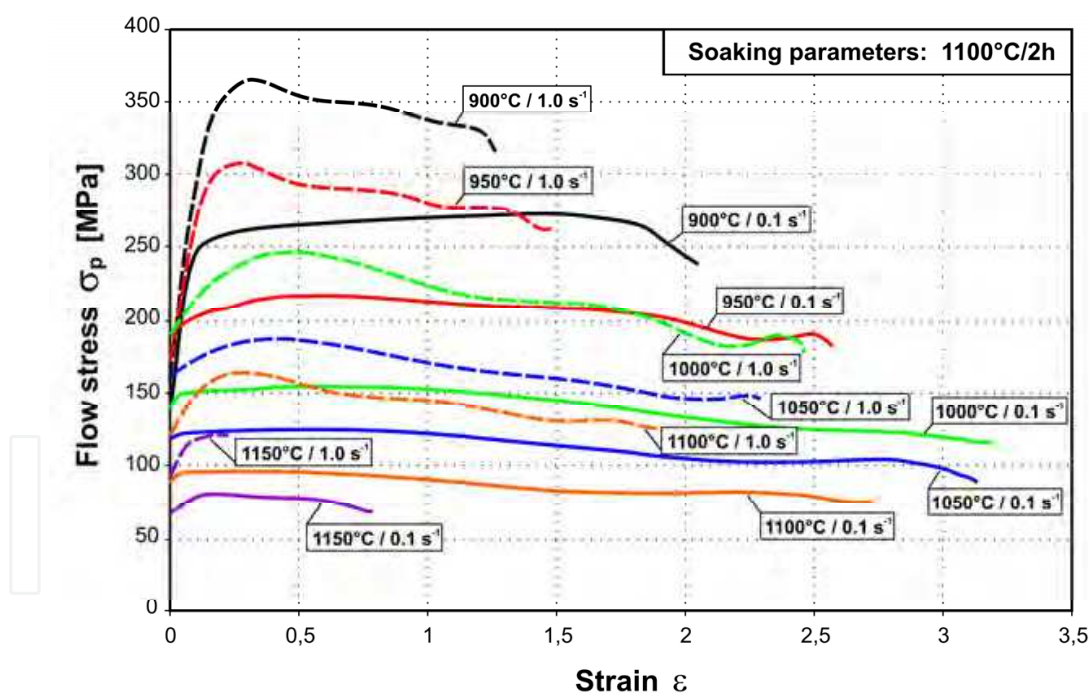
Fig. 4. The effect of deformation temperature on the flow stress of Fe-Ni alloy after initial soaking at 1100°C/2 h. Strain rate: 0.1 s^{-1} and 1.0 s^{-1}
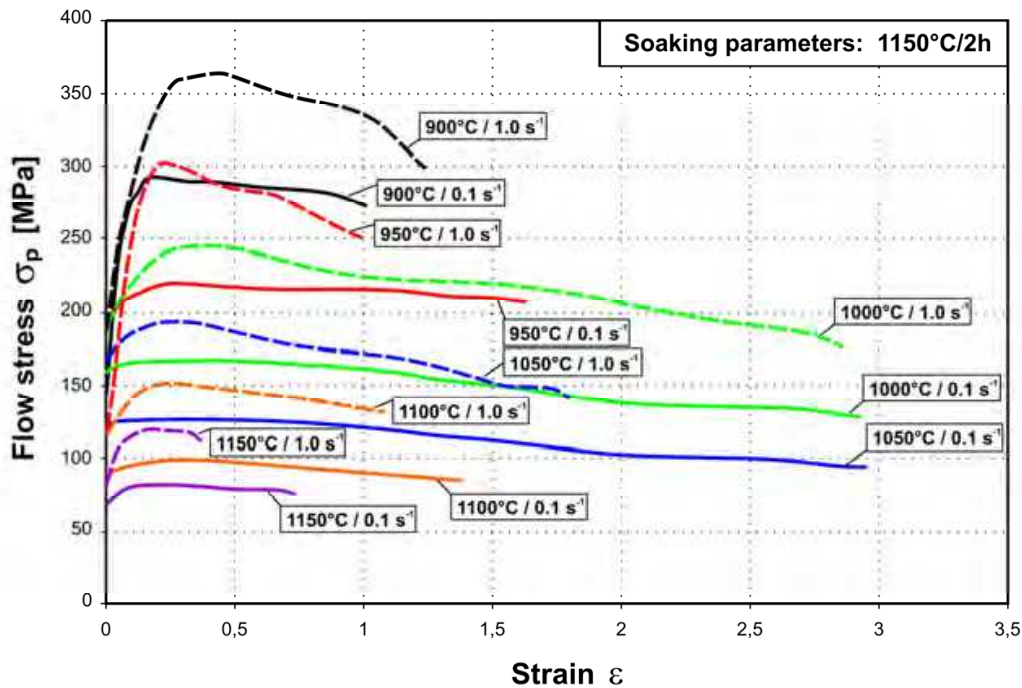
Fig. 5. The effect of deformation temperature on the flow stress of Fe-Ni alloy after initial soaking at 1150°C/2h. Strain rate: 0.1 s⁻¹ and 1.0 s⁻¹

An increase of the initial soaking temperature to 1150°C/2h significantly reduces the alloy deformability for the two strain rates, both at low and high deformation temperatures (Fig. 5). In this case, fairly high deformation values were obtained for the alloy in a narrow range of torsion temperatures, i.e. 1000÷1050°C. Such behavior of the alloy may be explained by a larger growth of austenite grains at this soaking temperature and, consequently, lower recovery and dynamic recrystallization rates.

The values determined for the maximum yield stress σ_{pp}, maximum deformation ε_p, stress until failure σ_f and threshold deformation ε_f depending on the temperature and strain rate are presented in Figs. 6-9. For the option of initial soaking at 1100°C/2h and torsion speed of 0.1 s⁻¹, the alloy under discussion shows a contiuous drop of σ_{pp} from values 277 MPa at a temperature of 900°C to the value of 81 MPa at 1150°C (Fig. 6). The threshold deformation ε_f rises initially together with the torsion temperature, reaching the maximum of (3.19/3.14) at 1000÷1050°C, and then falls (Fig. 8). An increase of the strain rate to 1.0 s⁻¹ results in an increase of σ_{pp} to maximum values of 367 MPa at the temperature of 900°C (Fig. 6) and a decrease of the threshold deformation to the maximum of 2.47/2.34 at 1000÷1050°C (Fig. 8).
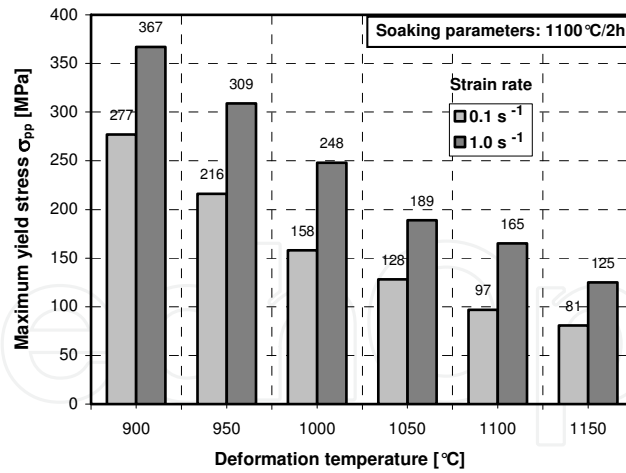
Fig. 6. The effect of deformation conditions on maximum flow stress. Initial alloy soaking: 1100°C/2 h
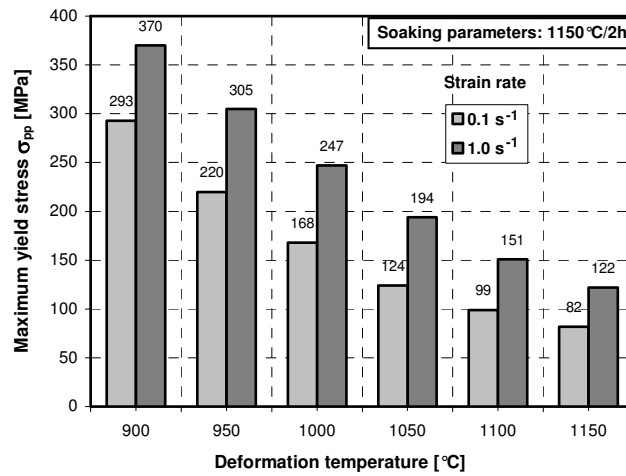
Fig. 7. The effect of deformation conditions on maximum flow stress. Initial alloy soaking: 1150°C/2 h
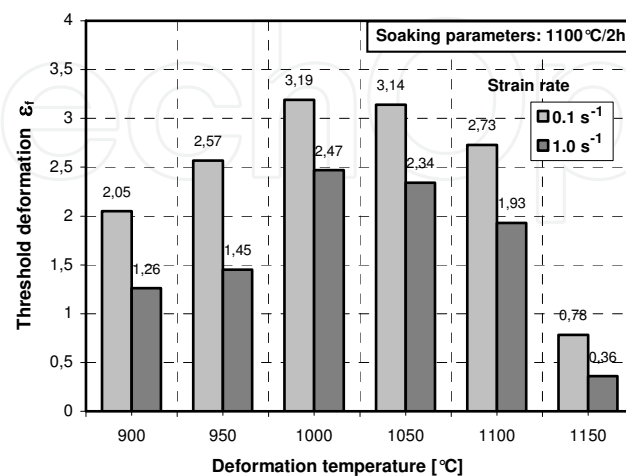
Fig. 8. The effect of deformation conditions on threshold deformation of the alloy. Initial soaking: 1100°C/2 h
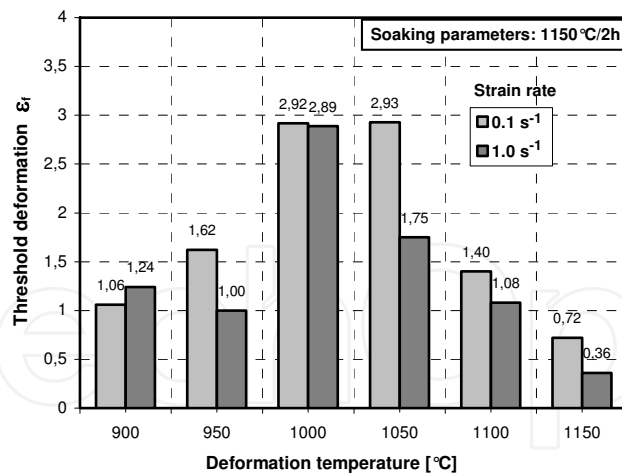
Fig. 9. The effect of deformation conditions on threshold deformation of the alloy. Initial soaking: 1150°C/2 h

An increase of the alloy initial soaking temperature to 1150°C/2h at a strain rate of 0.1 s⁻¹ results in a slight increase of σ_{pp} to maximum values of 293 MPa at 900°C (Fig. 7) and decrease of ε_f to the maximum of 2.92÷2.93 in the range of 1000÷1050°C (Fig. 9). An increase of the torsion speed to 1.0 s⁻¹ results in further increase of the σ_{pp} value to maximum values of 370 MPa at 900°C (Fig. 7), and decrease of ε_f to the maximum values of 2.89/1.75 at the temperature of 1000÷1050°C (Fig. 9).

The activation energy of the hot plastic deformation process Q was calculated by the means of a computer programme ENERGY 3.0 (Schindler et al., 1998). The activation energy, Q, necessary to initiate dynamic recrystallization in the Fe-Ni alloy, was determined on the basis of the linear dependencies presented in Fig. 10.
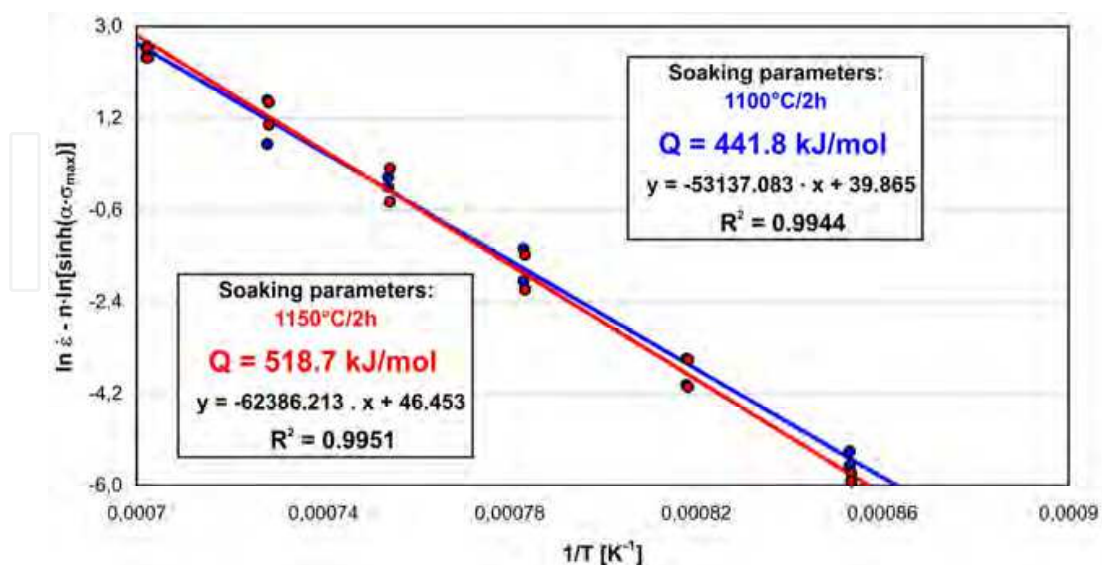
Fig. 10. The plot for determination of the activation energy for hot plastic deformation of the Fe-Ni alloy. Initial alloy soaking: 1100°C/2 h and 1150°C/2 h

The activation energy, Q, of hot plastic deformation for the Fe-Ni alloy depends on the temperature of initial soaking and equals as follows:

- Q = 441.8 [kJ/mol] – for initial alloy soaking 1100°C/2 h;
- Q = 518.7 [kJ/mol] – for initial alloy soaking 1150°C/2 h.

The higher value of the activation energy, Q, of hot plastic deformation for the alloy after initial soaking at 1150°C/2h can be justified by higher values of the maximum yield stress σ_{pp}, a larger growth of the initial austenite grain and a higher degree of matrix saturation with alloying elements.

The dependencies between maximum yield stress σ_{pp} and Zener Hollomon Z parameter are presented in Fig. 11. For both options of initial soaking, a power dependence (R^2 = 0,98) of the alloy yield stress was obtained as a function of the Z parameter. So determined function dependencies between the maximum yield stress σ_{pp} and the Z parameter had a form of power function:

- for the alloy after initial soaking 1100°C/2 h:

$$\sigma_{pp} = 0.43 \times Z^{0.151} \text{ [MPa]} \tag{14}$$

- for the alloy after initial soaking 1150°C/2 h:

$$\sigma_{pp} = 0.34 \times Z^{0.133} \text{ [MPa]} \tag{15}$$

Higher values of the Z parameter for the alloy after initial soaking at 1150°C/2h result from higher values of the plastic deformation activation energy Q.
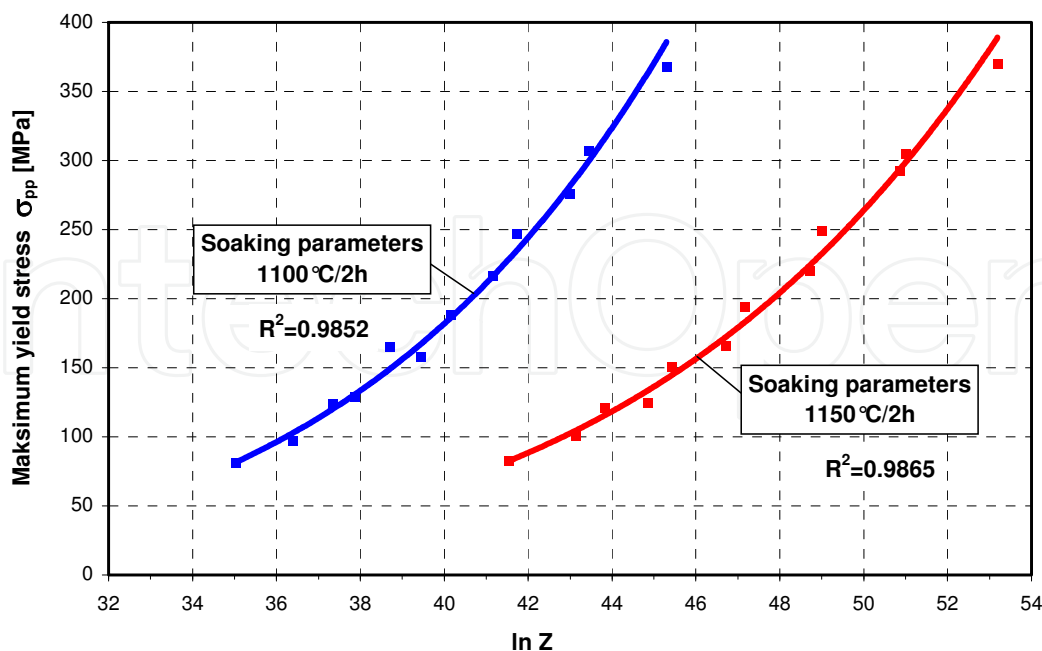
Fig. 11. Dependence of the maximum flow stress σ_{pp} on the Zener-Hollomon parameter Z. Initial alloy soaking: 1100°C/2 h and 1150°C/2 h

3.3 Microstructure of hot-deformed alloy

The recovery and dynamic recrystallization which occur in the Fe-Ni alloy during hot plastic deformation affect the size of the austenite grain. The results of investigations of the alloy microstructure after initial soaking at 1100°C/2h and deformation in a temperature range 900÷1150°C and a strain rate of 0.1 and 1.0 s^{-1} are presented in Figs. 12a-d.


a)   b)

c)   d)
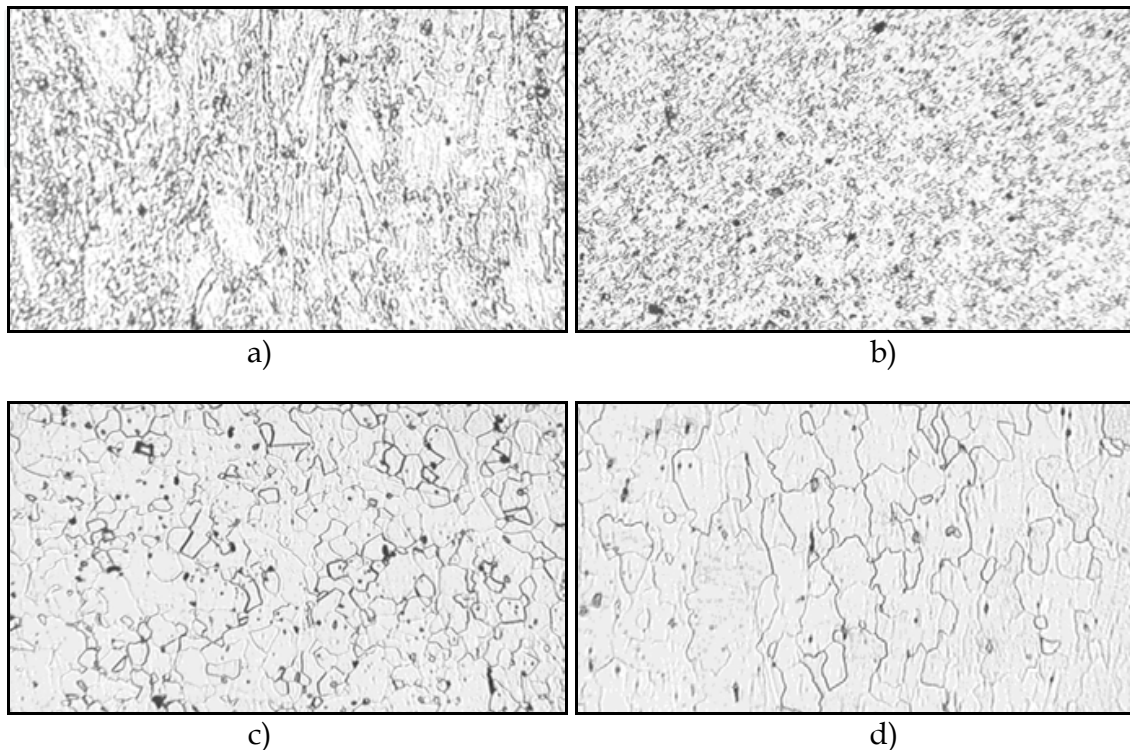
Fig. 12. The microstructure of the alloy after plastic deformation at: a) 900°C/1.0 s^{-1},
b) 950°C/0.1 s^{-1}, c) 1100°C/1.0 s^{-1}, d) 1150°C/0.1 s^{-1}. Initial soaking: 1100°C/2h

After deformation at 900°C for both of the torsion rates applied, the alloy structure is not completely recrystallized, which is indicated by the presence of primary elongated grains and fine recrystallized grains (Fig. 12a). At a torsion temperature in the range of 950÷1100°C, the alloy structure consisted of dynamically recrystallized grains (Fig. 12b and 12c). With an increasing deformation temperature, a gradual growth of the recrystallized grains was observed. The recrystallized grains were characterized by a deformed grain boundary line, which indicates an extensive cumulated deformation in the specimens. At the highest torsion temperature, 1150°C, some elongated grains of dynamically recrystallized austenite are observed in the alloy structure (Fig. 12d).

An increase of the initial soaking temperature of the alloy to 1150°C/2h results in increasing the initial austenite grain size and decreasing the kinetics of dynamic recovery and recrystallization for both of the analyzed strain rates (Figs. 13a-d). After deformation at 900°C/0.1 s^{-1} and 900÷950°C/1.0 s^{-1}, the alloy microstructure was not completely recrystallized and it was composed of deformed primary grains and dynamically recrystallized grains of small sizes (Fig. 13a and 13b). The new, fine recrystallized grains nucleated at primary grain boundaries, creating the so-called "necklace". Within the deformation temperature range from 950÷1000 to 1100°C, the alloy structure is fine-grained

and completely dynamically recrystallized (Fig. 13c). The highest deformation temperature of 1150°C induced deformation localization, as evidenced by the elongated dynamically recrystallized grains of varying sizes (Fig. 13d).
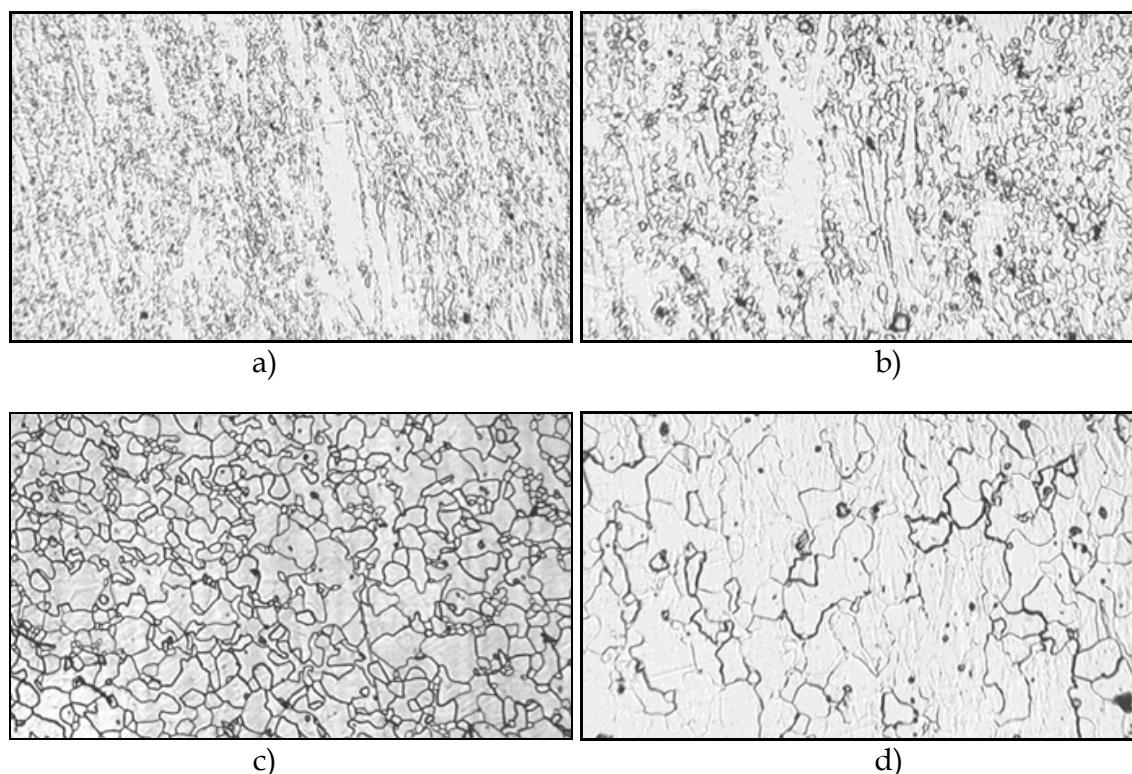

Fig. 13. The microstructure of the alloy after plastic deformation at: a) 900°C/1.0 s^{-1}, b) 950°C/0.1 s^{-1}, c) 1050°C/1.0 s^{-1}, d) 1150°C/0.1 s^{-1}. Initial soaking: 1150°C/2h

The results of a quantitative evaluation of the structure after initial soaking and deformation until failure in a temperature range of 900-1150°C and a strain rate of 0.1 and 1.0 s^{-1} are presented in Figs. 14-17. In the structure of the alloy after initial soaking 1100°C/2h and deformation in the investigated temperature range at a strain rate 0.1 s^{-1}, monotonous growth of the grain average area $\bar{A}$ is observed from a value 16 μm^2 at 900°C to 198 μm^2 at 1150°C (Fig. 14). Up to the deformation temperature of 1100°C, the dynamically recrystallized grains are approximately equiaxial ($\delta = 0.99 \div 1.12$), whereas at the highest torsion temperature, 1150°C, they are elongated ($\delta = 1.31$) (Fig. 15). An increase of the strain rate to 1.0 s^{-1} induces a certain reduction of the recrystallized grain size.

Also, in this case, in the investigated range of deformation temperatures, a monotonous growth of the grain average area $\bar{A}$ was observed, from 12 μm^2 at 900°C to 87 μm^2 at 1100°C (Fig. 14). In the analyzed range of torsion temperatures of 900÷1100°C, the dynamically recrystallized grains are approximately equiaxial ($\delta = 1.00 \div 1.09$) (Fig. 15).
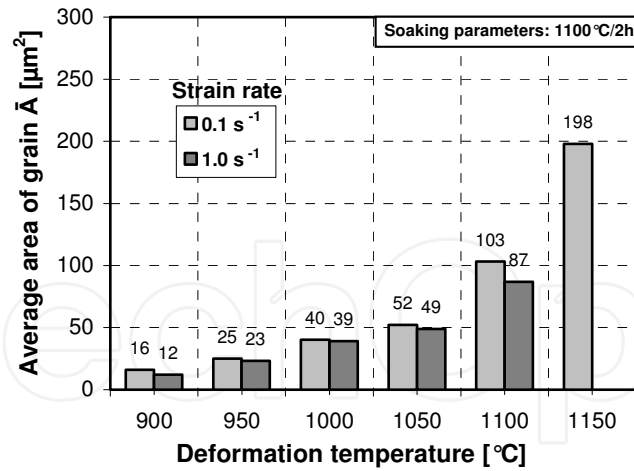
Fig. 14. The effect of deformation temperature on the average area of recrystallized grain after torsion at a rate of 0.1 and 1.0 s^{-1}. Initial soaking: 1100°C/2h
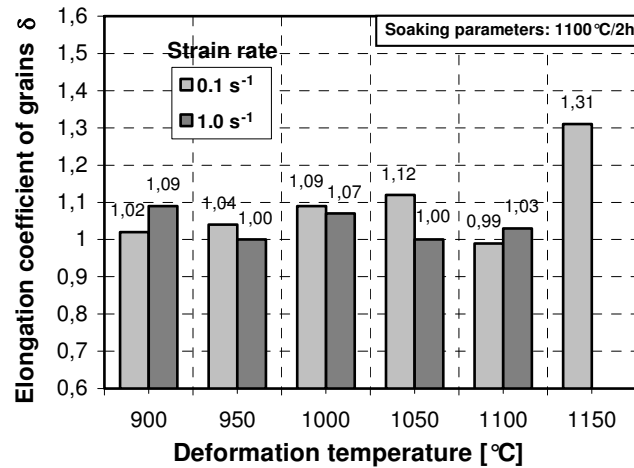

Fig. 15. The effect of deformation temperature on the elongation coefficient of recrystallized grain after torsion at a rate of 0.1 and 1.0 s^{-1}. Initial soaking: 1100°C/2h
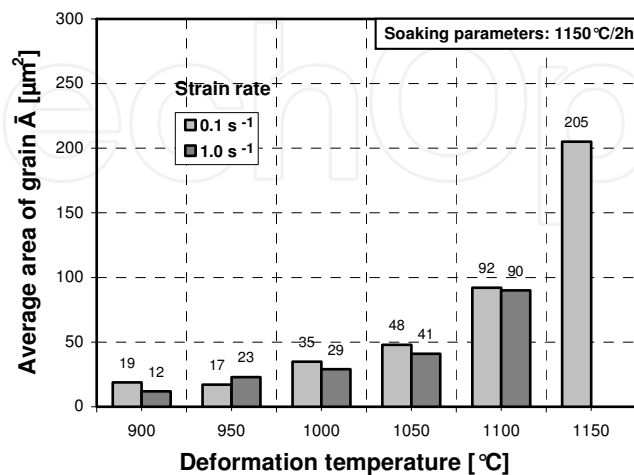
Fig. 16. The effect of deformation temperature on the average area of recrystallized grain after torsion at a rate of 0.1 and 1.0 s^{-1}. Initial soaking: 1150°C/2h
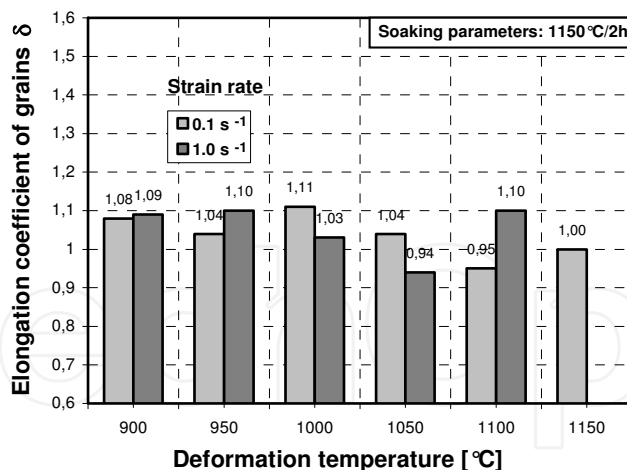
Fig. 17. The effect of deformation temperature on the elongation coefficient of recrystallized grain after torsion at a rate of 0.1 and 1.0 s^{-1}. Initial soaking: 1150°C/2h

An increase of the initial soaking temperature to 1150°C/2h and alloy deformation within the range of 900÷1150°C at a rate of 0.1 s^{-1} induces a similar reduction in size of the grain plane section area from 19 µm^2 at 900°C to 205 µm^2 at 1150°C (Fig. 16). An increase of the strain rate of samples to 1.0 s^{-1} within the deformation temperature range of 900÷1100°C causes a further reduction in the grain average area within the range from 12 to 90 µm^2. For both strain rates, the grains after dynamic recrystallization are approximately equiaxial (δ = 0.94÷1.11) (Fig. 17).

A comparison of the size of recrystallized grain in the Fe-Ni alloy after deformation at a strain rate of 0.1 and 1.0 s^{-1} for two variants of initial soaking at 1100°C/2 h and 1150°C/2 h is presented in Fig. 18 and 19. After deformation at a strain rate of 0.1 s^{-1} within the temperature range of 900÷1150°C for both variants of initial soaking, a similar grain size $\bar{A}$ was obtained in the range from 16 to 205 µm^2 (Fig. 18). A higher strain rate of 1.0 s^{-1} within the temperature range of 900÷1100°C allows obtaining a slightly higher degree of grain refining in the range from 12 to 90 µm^2 (Fig. 19). Thus, it can be concluded that the initial microstructure of an alloy after initial soaking has no significant influence on the size of recrystallized grain after plastic deformation.
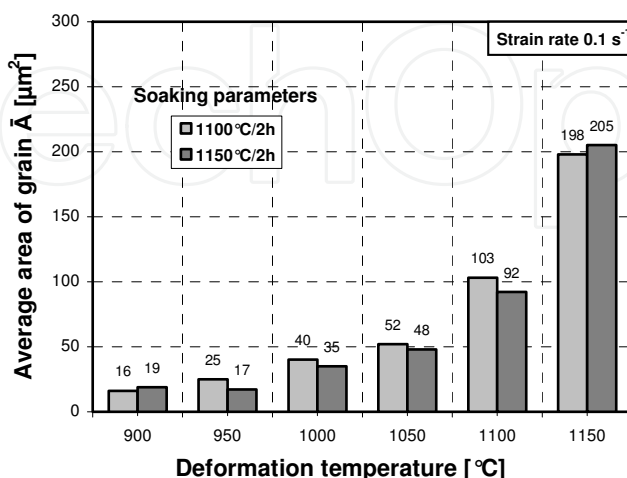
Fig. 18. The effect of deformation temperature on the average area of recrystallized grain after initial soaking of the alloy at 1100°C/2 h and 1150°C/2 h
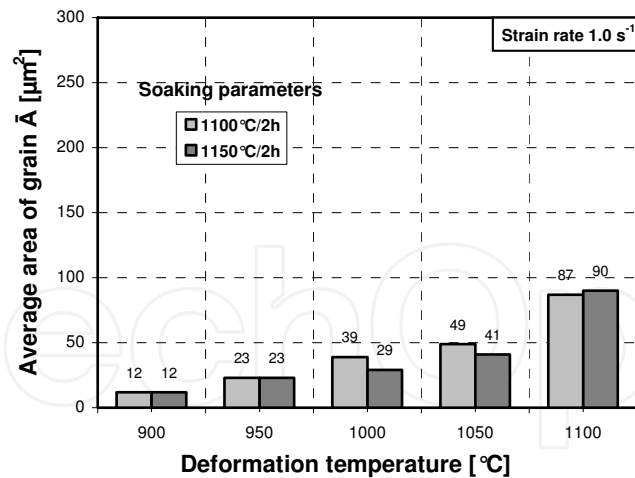
Fig. 19. The effect of deformation temperature on the average area of recrystallized grain after initial soaking of the alloy at 1100°C/2 h and 1150°C/2 h

The average grain plane section area of samples deformed under the same conditions but with a different initial grain size after initial soaking is similar. The average size of recrystallized austenite grain depends mainly on the deformation temperature and, to a lesser degree, on the strain rate applied for the alloy (Fig. 20 and 21).
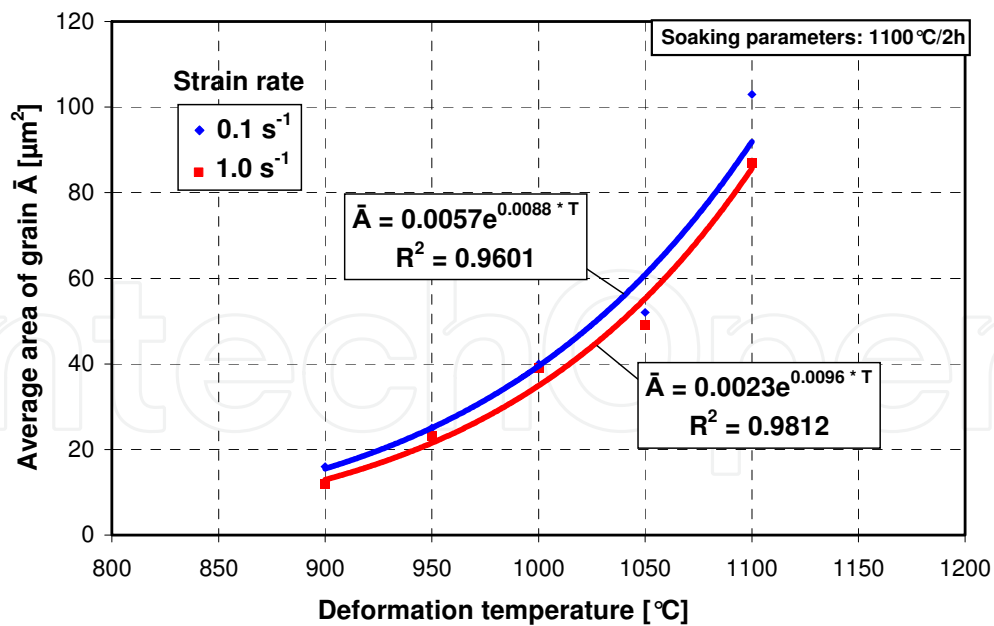

Fig. 20. Relationship between the average grain area after recrystallization versus deformation temperature and strain rate. Initial alloy soaking: 1100°C/2 h
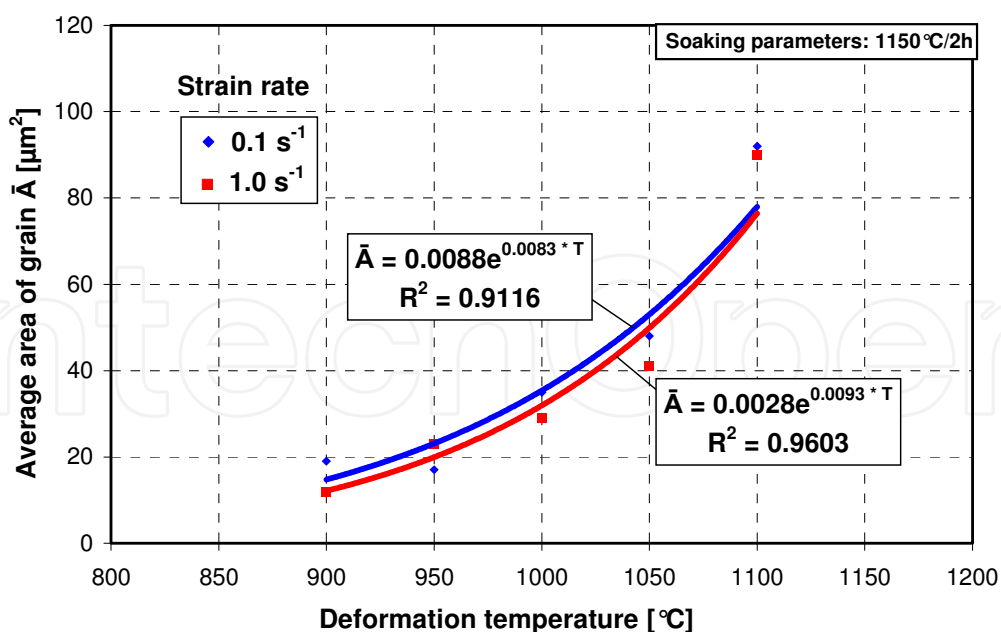
Fig. 21. Relationship between the average grain area after recrystallization versus
deformation temperature and strain rate. Initial alloy soaking: 1150°C/2 h

An assessment of the degree of influence of the deformation temperature and strain rate on the
average grain plane section area of the recrystallized Fe-Ni alloy was obtained after
introducing the Zener-Hollomon Z parameter. As appears from the dependencies developed,
the fine-grained microstructure of the alloy after deformation was obtained more easily after
initial soaking at a temperature of 1100°C/2h when compared to soaking at 1150°C/2 h (Fig.
22). This is evidenced by lower Z parameter values for the deformation after initial soaking at
1100°C/2 h: a low strain rate and a moderate deformation temperature.
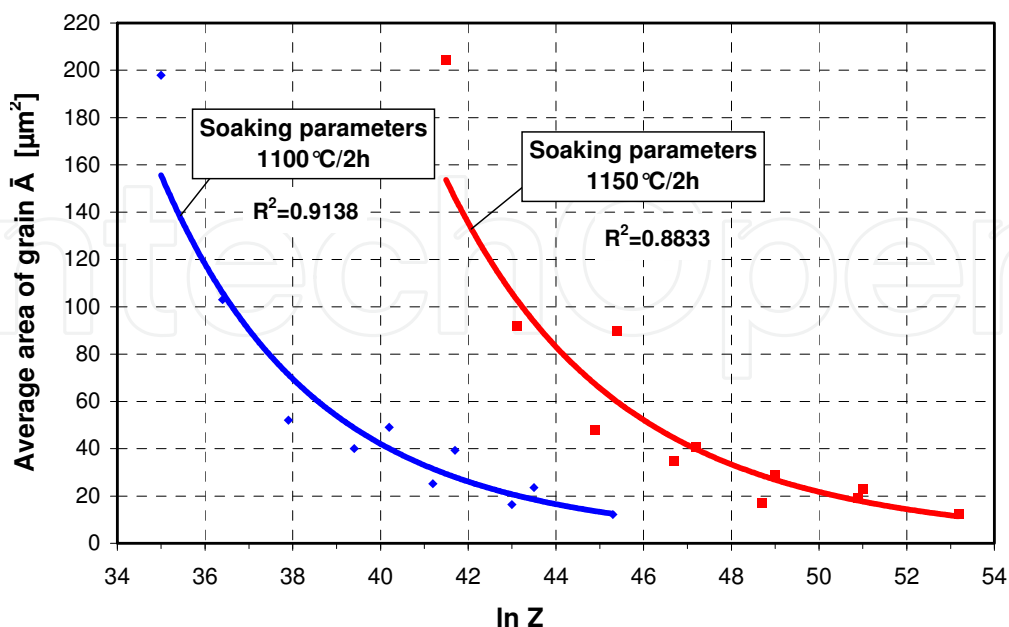
Fig. 22. Relationship between the Zener-Hollomon parameter and the average grain area
after recrystallization. Initial alloy soaking: 1100°C/2 h and 1150°C/2 h

For both variants of initial soaking of the alloy, relationships were determined between the average plane section area of the recrystallized grain $\bar{A}$ and the Z parameter (eq. 16 and 17):

- for the alloy after initial soaking 1100°C/2h:

$$\bar{A} = 9.3 \times 10^5 \times Z^{-0.250} \text{ [µm}^2\text{]} \tag{16}$$

- for the alloy after initial soaking 1150°C/2h:

$$\bar{A} = 2.0 \times 10^6 \times Z^{-0.224} \text{ [µm}^2\text{]} \tag{17}$$

The determined relationships are essential where the critical value of a significance test for the direction factor of regression line "p" is less than 0.05. In the analyzed case, the "p" factor value for both variants of initial soaking of the alloy, i.e. at 1100°C/2h and 1150°C/2h, equaled 3.08×10^{-5} and 5.03×10^{-5}, respectively, which indicates the significance of the determined relationships.

3.4 Substructure of hot-deformed alloy

The recovery and dynamic recrystallization processes during hot plastic deformation of the Fe-Ni alloy cause changes in the dislocation and subgrain substructures. An analysis of the microscopic examination results allows affirming that the nature and extent of changes in the alloy substructure was dependent on the deformation temperature and strain rate, and the conditions of initial soaking. After initial soaking (1100°C/2 h) and deformation at a temperature of 900°C and a rate of 0.1 and 1.0 s^{-1}, effects of dynamic recovery and dynamic recrystallization (Fig. 23 and 24) were observed in the alloy microstructure. In grain areas with major defects of the austenite, a cellular dislocation substructure and subgrains with different dislocation densities were formed.
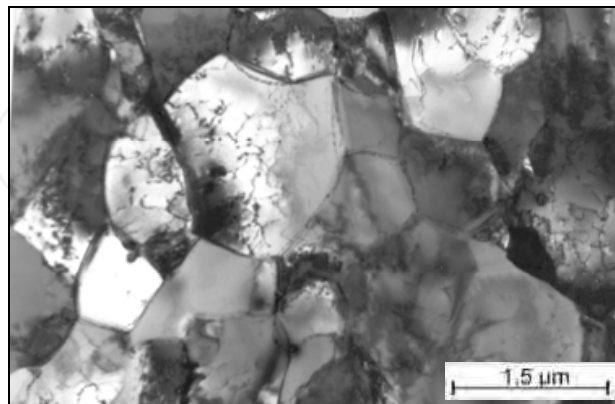
Fig. 23. Alloy microstructure after soaking at 1100°C/2 h and deformation at 900°C/0.1 s^{-1}. Subgrains and recrystallized grains
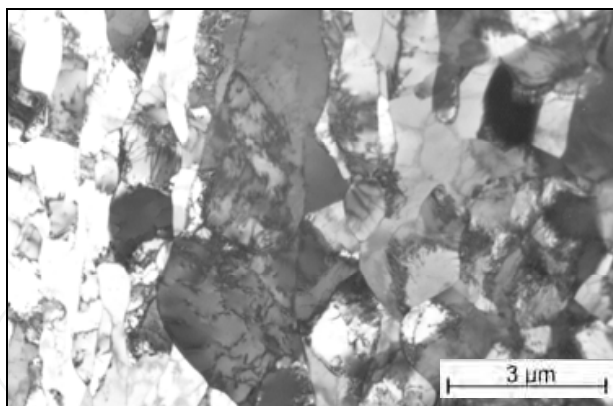
Fig. 24. Alloy microstructure after soaking at 1100°C/2 h and deformation at 900°C/1.0 s⁻¹.
Subgrain structure formation

At a higher deformation temperature, e.g. 950°C, the proceeding recovery processes were accompanied by intensive dynamic recrystallization (Fig. 25 and 26). In the alloy substructure, dynamically recrystallized grains were observed next to the subgrains (Fig. 25). In the samples deformed at a higher rate, 1.0 s⁻¹, at this temperature the fraction and size of dynamically recrystallized microregions increase (Fig. 26).

The alloy deformed within the temperature range of 1000÷1050°C is characterized by a microstructure typical of a dynamically recrystallized material (Fig. 27 and 28). The austenite microstructure is composed predominantly of recrystallized grains free of dislocations (Fig. 27). Further perfecting of the substructure is observed in the neighbouring subgrains, as evidenced by equiaxiality of the subgrains and the decreasing density of dislocations inside them (Fig. 28). It was found that a higher strain rate (1.0 s⁻¹) leads to a growth of the subgrain and a reduction of the dislocation density.
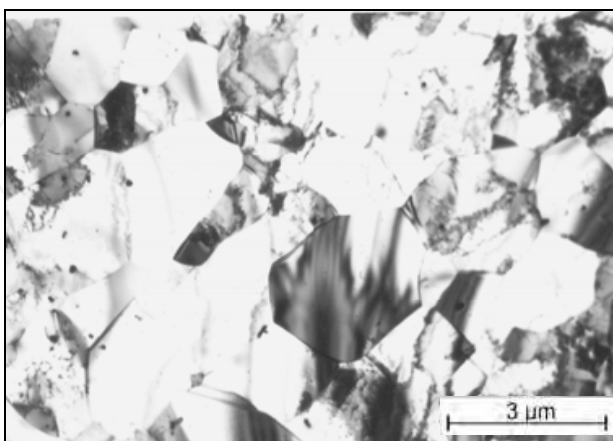
Fig. 25. Alloy microstructure after soaking at 1100°C/2 h and deformation at 950°C/0.1 s⁻¹.
Subgrains and recrystallized grains
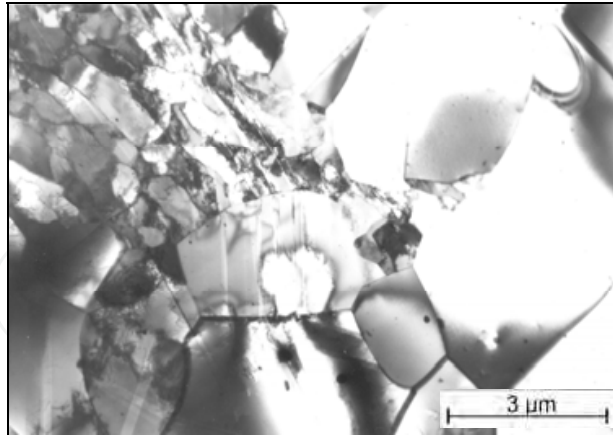
Fig. 26. Alloy microstructure after soaking at 1100°C/2 h and deformation at 950°C/1.0 s⁻¹. Regions of recrystallized austenite and subgrains
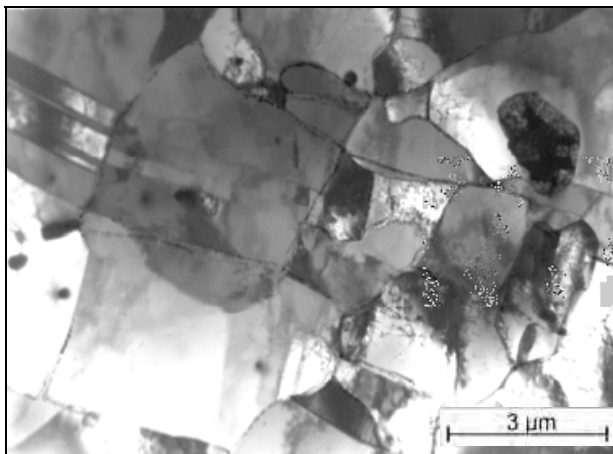
Fig. 27. Alloy microstructure after soaking at 1100°C/2 h and deformation at 1000°C/0.1 s⁻¹. Recrystallized grains with twins and subgrains
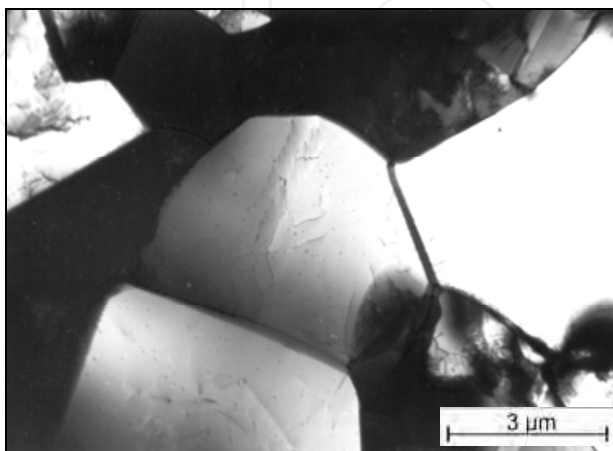

Fig. 28. Alloy microstructure after soaking at 1100°C/2 h and deformation at 1050°C/1.0 s⁻¹. The process of further perfecting of the subgrain structure

In the alloy substructure, after deformation at the highest temperature of 1100÷1150°C, a reincrease of the dislocation density and repolygonization were observed (Fig. 29). At a higher strain rate of 1.0 s^{-1}, areas with recrystallized grain free of dislocations are dominant in the alloy substructure (Fig. 30).

An increase of the initial soaking temperature to 1150°C/2h inhibits the dynamic recovery and recrystallization processes (Fig. 31 and 32). In the regions with austenite subgrain after deformation at a temperature of 900°C at a rate of 0.1 s^{-1}, deformation microtwins appear (Fig. 31). The subgrains being formed, especially at a high strain rate of 1.0 s^{-1}, have an elongated shape and different dislocation densities (Fig. 32).

At a higher deformation temperature, e.g. 1000°C, and a strain rate of 0.1 and 1.0 s^{-1}, the alloy substructure reconstruction is inhomogeneous. It is characterized by the presence of areas where structural changes are inhibited and accelerated (Fig. 33 and 34).

Effects of dynamic recovery (Fig. 33) and dynamic recrystallization (Fig. 34) were found there. The growth of new grains in the dynamic recrystallization process proceeded through the coalescence of subgrains and their subsequent growth (Fig. 35). The bending of the grain boundary towards areas with a higher dislocation density indicates the direction of the boundary movement. The principal mechanism of the coalescence includes reactions between dislocations which lead to disappearance of the dislocation boundary and formation of grain from the combination of several neighboring subgrains.

The dislocation density in the subgrain area does not decrease significantly when increasing the deformation temperature to 1100°C compared to a lower deformation temperature (Fig. 36 and 37). The dynamic deformation phenomena are accompanied by a continuous process of structural reconstruction of the material, i.e. repolygonization. It consists in re-saturation of subgrains with dislocations and their rearrangement together with the creation of new subboundaries and walls of a polygonal type (Fig. 36).

Deformation of the alloy at a higher rate of 1.0 s^{-1} was accompanied in the substructure by dislocation rearrangement with the formation of polygonal walls and a cellular substructure (Fig. 37). The phenomenon of repolygonization in the austenite grains was observed at the highest deformation temperature (1100÷1150°C).
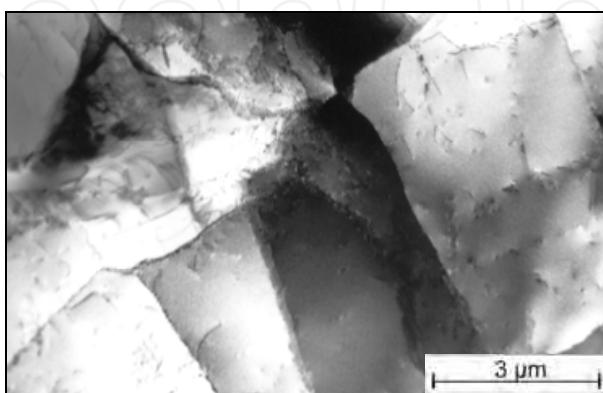
Fig. 29. Alloy microstructure after soaking at 1100°C/2 h and deformation at 1100°C/0.1 s^{-1}. The effects of repolygonization in austenite subgrains
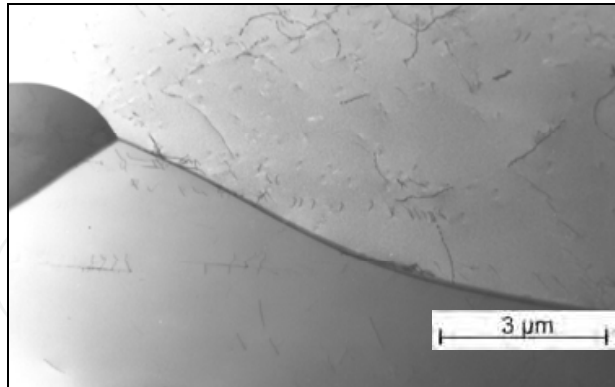
Fig. 30. Alloy microstructure after soaking at 1100°C/2 h and deformation at 1100°C/1.0 s^{-1}. Large austenite subgrains with a low dislocation density
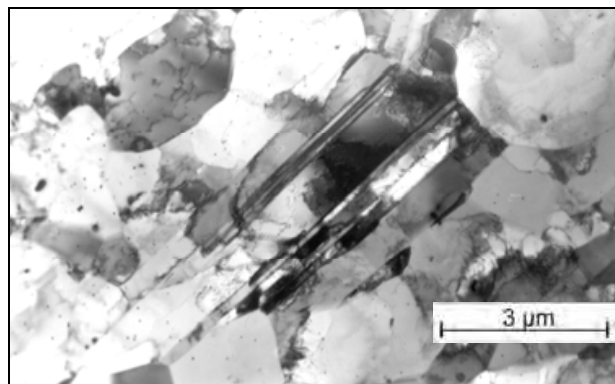

Fig. 31. Alloy microstructure after soaking at 1150°C/2 h and deformation at 900°C/0.1 s^{-1}. Subgrain structure and grains with microtwins
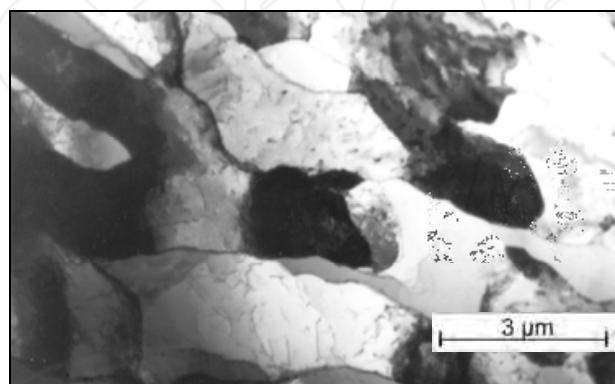

Fig. 32. Alloy microstructure after soaking at 1150°C/2 h and deformation at 900°C/1.0 s^{-1}. Non-equiaxed, austenite subgrains
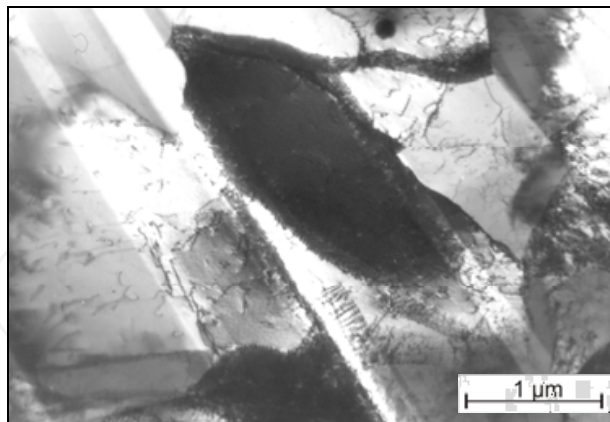
Fig. 33. Alloy microstructure after soaking at 1150°C/2 h and deformation at 1000°C/0.1 s⁻¹.
The effects of polygonization and deformation microtwins
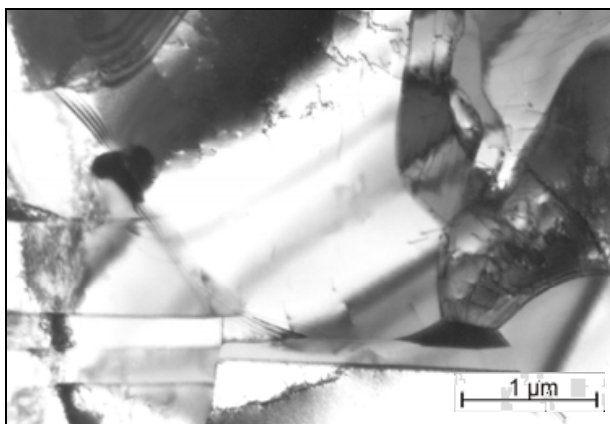
Fig. 34. Alloy microstructure after soaking at 1150°C/2 h and deformation at 1000°C/1.0 s⁻¹.
The grains after dynamic recrystallization
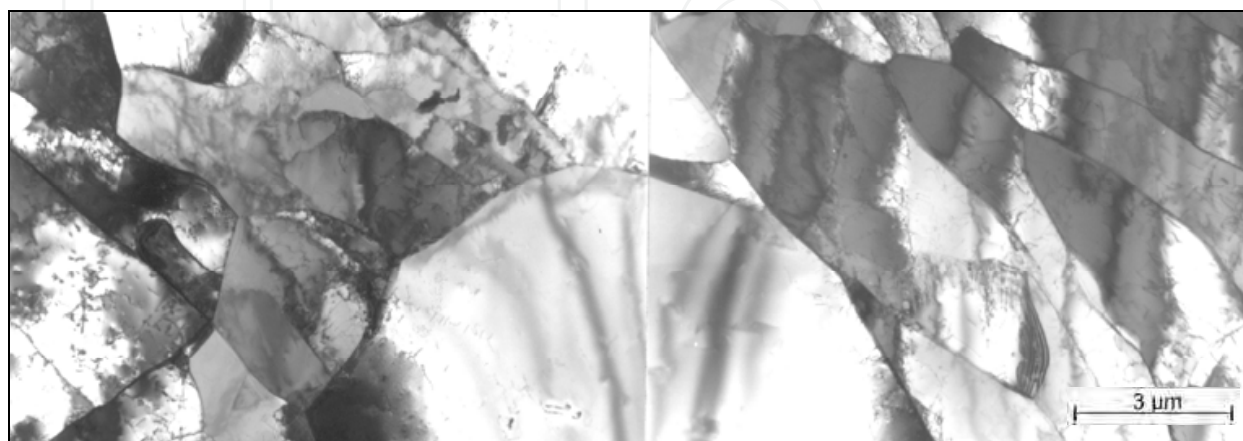
Fig. 35. Alloy microstructure after soaking at 1150°C/2 h and deformation at 1000°C/0.1 s⁻¹.
The recrystallized grain formation as a result of coalescence of subgrains
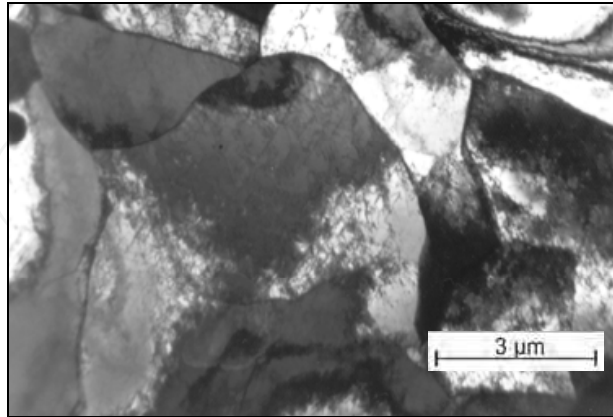
Fig. 36. Alloy microstructure after soaking at 1150°C/2 h and deformation at 1100°C/0.1 s^{-1}. The formed subgrain structure with dislocations
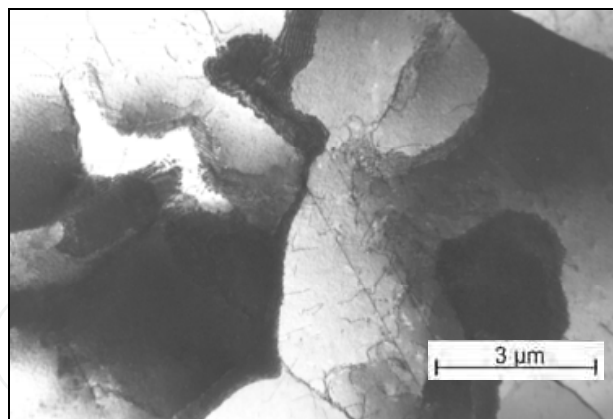
Fig. 37. Alloy microstructure after soaking at 1150°C/2 h and deformation at 1100°C/1.0 s^{-1}. Austenite repolygonization and a cellular dislocation structure

The course of changes in the subgrain sizes depending on the temperature deformation and strain rate for the two variants of initial soaking of the alloy is shown in Fig. 38 and 39. It was found that an increase in the alloy deformation temperature from 900 to 1150°C results in a growth of the subgrain.
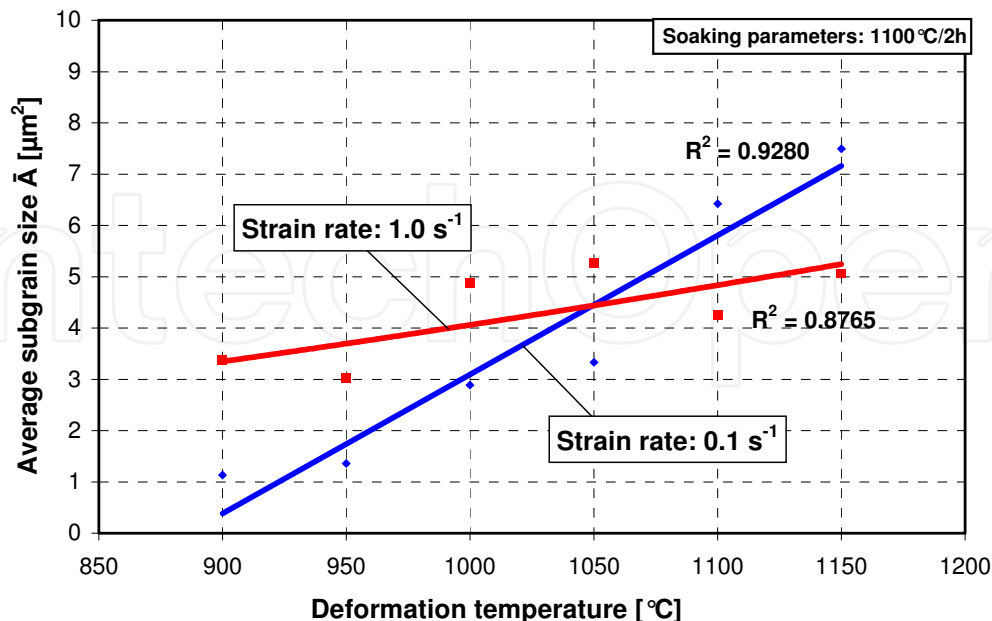
Fig. 38. The effect of temperature deformation and strain rate on the average subgrain size. Initial alloy soaking: 1100°C/2 h
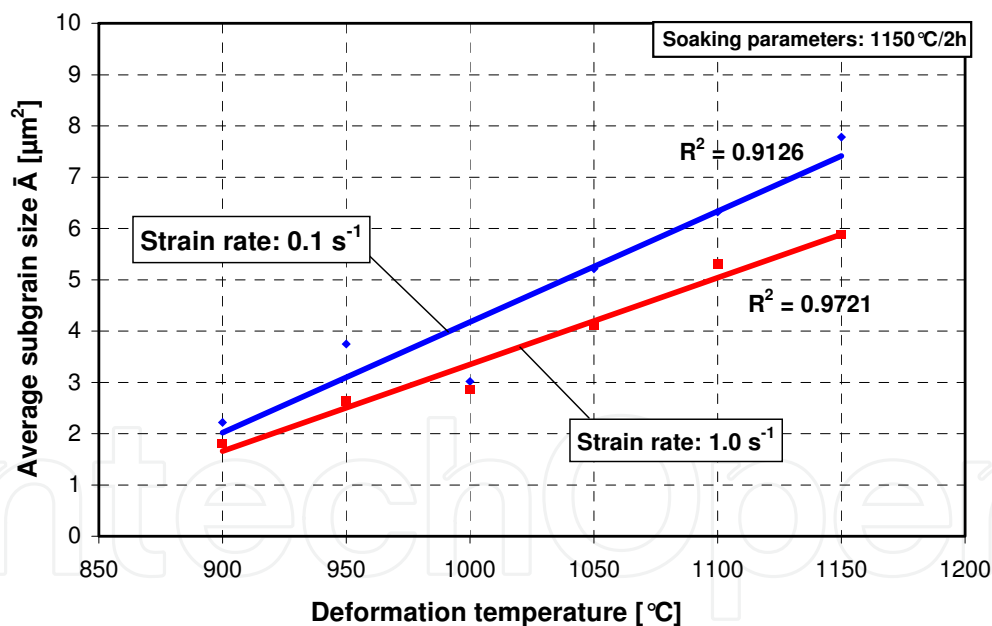

Fig. 39. The effect of temperature deformation and strain rate on the average subgrain size. Initial alloy soaking: 1150°C/2 h

However, no influence was observed of the conditions of initial soaking on the subgrain size. The average area of the subgrain plane section $\bar{A}$ varied within the range from 1.0 µm² to 7.8 µm² for both variants of initial soaking. The influence of the strain rate on the subgrain size was more significant, in particular for the initial soaking at 1100°C/2 h (Fig. 38). More intensive changes in the subgrain size were observed at a low strain rate of 0.1 s⁻¹, which can be explained by a higher cumulative deformation in the samples.

The dislocation density depending on the deformation temperature and strain rate for the two variants of initial soaking of the alloy is shown in Fig. 40 and 41. An increase of the deformation temperature was accompanied by a decreasing dislocation density. No significant influence was found of the initial soaking parameters on the dislocation density.
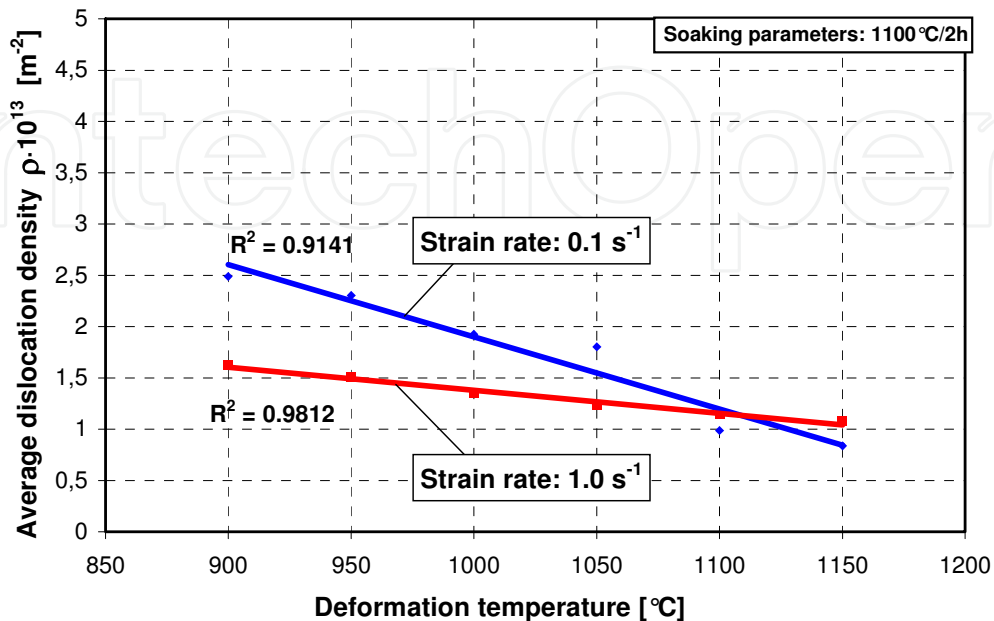

Fig. 40. The effect of temperature deformation and strain rate on the average dislocation density. Initial alloy soaking: 1100°C/2 h
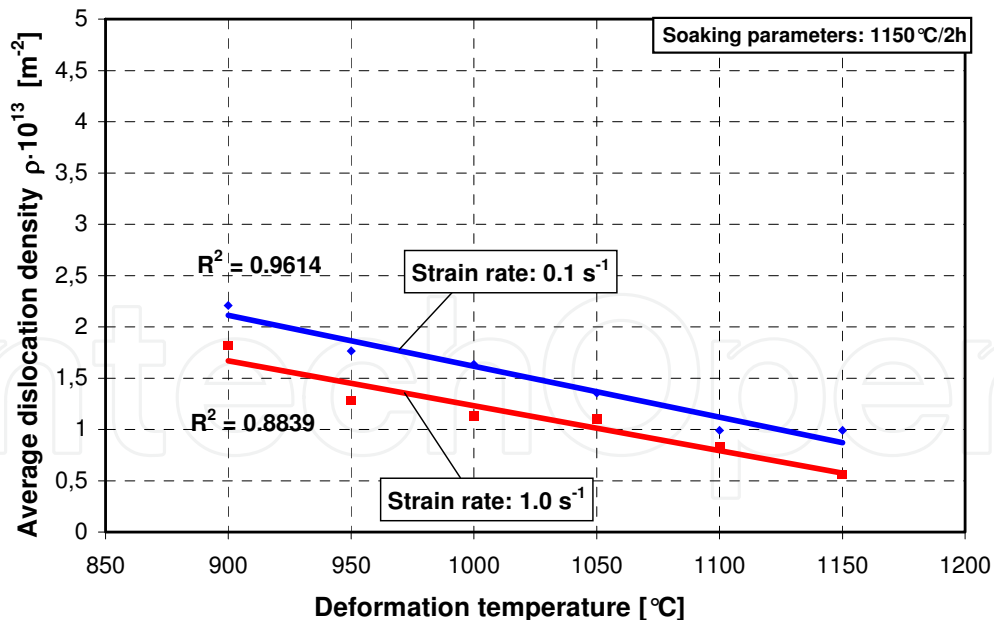

Fig. 41. The effect of temperature deformation and strain rate on the average dislocation density. Initial alloy soaking: 1150°C/2 h

For both variants of initial soaking, the dislocation density varied within a narrow range from 0.8×10^{13} m^{-2} to 2.5×10^{13} m^{-2}. The gradual reduction in the dislocation density observed in the samples as the deformation temperature increased from 900 to 1150°C shows a

continuous process of substructure reconstruction and redeformation. For both variants of initial soaking of the alloy, higher dislocation densities were obtained for the lower strain rate (0.1 s^{-1}), which can be explained by a higher cumulative deformation in the material.

4. Summary

The work analyzes the relationships between the conditions of hot plastic deformation and deformability and microstructure of an austenitic Fe-Ni superalloy precipitation-strengthened by phase γ' type. The hot torsion tests carried out in the range of temperature of $900 \div 1150°C$, at a strain rate of 0.1 s^{-1} and 1.0 s^{-1} allowed determining the influence of the initial soaking conditions and deformation parameters on technological plasticity of the Fe-Ni superalloy, as well as on the strengthening and structure reconstruction processes. It was found that optimal values of the maximum yield stress σ_{pp} and threshold deformation ε_f, as well as the required fine-grain microstructure, were obtained for the alloy after initial soaking at $1100°C/2$ h and deformation at a rate of 0.1 s^{-1} in the temperature range of $1050 \div 950°C$. The increase of yield stress, σ_{pp}, and the decrease of deformability of the alloy, ε_f, as the initial soaking temperature was rising up to $1150°C/2$ h, with the deformation rate increasing to 1.0 s^{-1}, was associated with a growth of the initial grain size and the degree of austenite saturation with alloying elements. As a result of these processes, the stacking fault energy (SFE) of the austenite increased and so did the ability of the material to strengthen. This, in turn, led to an increase of activation energy of the hot plastic deformation process from the value $Q = 441.8$ kJ/mol (after initial soaking at $1100°C/2$ h) to $Q = 518.7$ kJ/mol (after initial soaking at $1150°C/2$ h).

An analysis of the flow curves and the examination results of the Fe-Ni alloy microstructure and substructure revealed dynamic recovery, recrystallization and repolygonization, occurring consecutively in the course of hot deformation. None of the detected stages of changes in the alloy structure constituted an independent process. Their course depended on both, the deformation parameters (T, $\dot{\varepsilon}$) and the initial soaking conditions. The growth of new grains in the dynamic recrystallization process took place through coalescence of subgrains and their subsequent growth. For both variants of initial soaking of the alloy, the analyzed quantitative indicators of the substructure depended fundamentally on the deformation temperature and, to a lesser degree, on the strain rate. The average size of subgrains $\bar{A}$ increased from 1.0 µm^2 to 7.8 µm^2 as the deformation temperature rose from $900°C$ to $1150°C$. The average dislocation density ρ decreased gradually in the range from 2.5×10^{13} m^{-2} to 0.8×10^{13} m^{-2} as the deformation temperature rose in the range of $900 \div 1150°C$.

The dynamic recrystallization proceeding in the Fe-Ni alloy during hot plastic deformation caused high refinement of the material structure. The average area $\bar{A}$ of recrystallized grains increased as the deformation temperature rose and it changed in the analyzed range of deformation parameters from 16 µm^2 to 205 µm^2, which, with reference to the initial grain size, meant refinement of the alloy structure of the order of $10 \div 370\times$. The average size of recrystallized austenite grain depended mainly on the deformation temperature and, to a lesser degree, on the strain rate. No significant influence was found of the initial grain size on the size of the dynamically recrystallized grain after plastic deformation. The existence of an exponential dependence between the average area of recrystallized austenite grain and the deformation temperature, as well as of an involutive dependence on the Zener-Hollomon parameter Z was shown.

5. Acknowledgment

6. References

Bywater K.A. & Gladman T. (1976). Influence of composition and microstructure on hot workability of austenitic stainless steels, *Metals Technology*, Vol. 3 (1976), pp. 358-368

Cwajna J.; Maliński M. & Szala J. (1993). The grain size as the structural criterion of the polycrystal quality evaluation, *Materials Engineering*, Vol. XIV (1993), pp. 79-88

Ducki K.J.; Hetmańczyk M. & Kuc D. (2006). Quantitative description of the structure and substructure of hot-deformed Fe-Ni austenitic alloy, *Materials Science Forum*, Vol. 513 (2006), pp. 51-60

Ducki K.J. (2010). Microstructural aspects of deformation, precipitation and strengthening processes in austenitic Fe-Ni superalloy. *Monograph. Copyright by Silesian University of Technology* (2010), pp. 1-136, ISBN 978-83-7335-721-1

Hadasik E. (2005). Methodology for determination of the technological plasticity characteristics by hot torsion test. *Archives of Metallurgy and Materials*, Vol. 50 (2005), pp. 729-746

Hansen N. (1998). Microstructure and properties of deformed metals, *Materials Engineering*, Vol. XIX (1998), pp. 108-115

Härkegård G. & Guédou J.Y. (1998). Disc Materials for Advanced Gas Turbines, Proceedings of the 6th Liége Conference: *Materials for Advanced Power Engineering*, 1998, pp. 913-931

Head A.K.; Humble P.; Clarebrough L.M.; Morton A.L. & Forwood C.T. (1973). Computed Electron Micrographs and Defects Identification, In: *Defects in Crystalline Solids*, Amelinckx S., Gevers R., Nihoul G. (Ed.), 1973, pp. 39-47

Klaar H.J.; Schwaab P. & Österle W. (1992). Round Robin Investigations into the Quantitative Measurement of Dislocation Density in the Electron Microscope, *Praktische Metallographie*, Vol. 29 (1992) (1), pp. 3-26

Kohno M.; Yamada T.; Suzuki A. & Ohta S. (1981). Heavy disk of heat resistant alloy for gas turbine, *Internationale Schmiedetagung 1981*, *Verein Deutscher Eisenhüttenleute*, Düsseldorf, Vol. 12 (1981), pp. 4.1.1-4.1.22

Koul A.K.; Immarigeon J.P. & Wallace W. (1994). Microstructural control in Ni-base superalloys, In: *Advances in high temperature structural materials and protective coatings*, National Research Council of Canada, Ottawa, 1994, pp. 95-125

McQueen H.J. & Ryan N.D. (2002). Constitutive analysis in hot working, *Materials Science and Engineering*, Vol. A322 (2002), pp. 43-63

Schindler I. & Bořuta J. (1998). Utilization Potentialities of the Torsion Plastometer. *Published by Department of Mechanics and Metal Forming, Silesian University of Technology* (1998) pp. 1-106, ISBN 83-910722-0-7

Sellars C.M. (1998). Role of computer modelling in thermomechanical processing, *Materials Engineering*, Vol. XIX (1998), pp. 100-107

Szala J. (1997). Computer program Quantitative Metallography, *Edited by Department of Materials Science, Silesian University of Technology* (1997)

Zener C. & Hollomon J.H. (1944). Plastic flow and rupture of metals, *Transactions of the ASM*, Vol. 33 (1944), pp. 163-235

Zhou L.X. & Baker T.N. (1994). Effects of strain rate and temperature on deformation behaviour of IN 718 during high temperature deformation, *Materials Science and Engineering*, Vol. A177 (1994), pp. 1-9
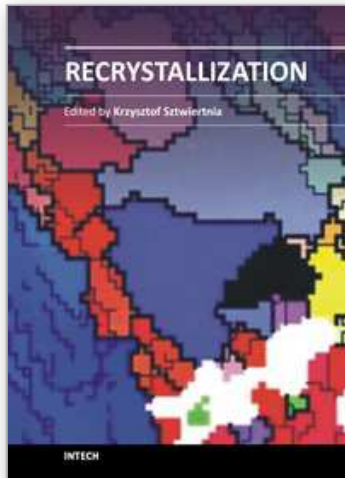
Recrystallization

Edited by Prof. Krzysztof Sztwiertnia

Recrystallization shows selected results obtained during the last few years by scientists who work on recrystallization-related issues. These scientists offer their knowledge from the perspective of a range of scientific disciplines, such as geology and metallurgy. The authors emphasize that the progress in this particular field of science is possible today thanks to the coordinated action of many research groups that work in materials science, chemistry, physics, geology, and other sciences. Thus, it is possible to perform a comprehensive analysis of the scientific problem. The analysis starts from the selection of appropriate techniques and methods of characterization. It is then combined with the development of new tools in diagnostics, and it ends with modeling of phenomena.

How to reference

In order to correctly reference this scholarly work, feel free to copy and paste the following:

INTECH

open science | open minds